ELSEVIER

Journal of Nuclear Materials 275 (1999) 125–137

journal of nuclear materials

www.elsevier.nl/locate/jnucmat

The influence of neutron irradiation on the fatigue performance of OFHC copper and a dispersion strengthened copper alloy

B.N. Singh[a,*], J.F. Stubbins[b], P. Toft[a]

[a] *Materials Research Department, Risø National Laboratory, 4000 Roskilde, Denmark*
[b] *Department of Nuclear Engineering, University of Illinois at Urbana-Champaign, Urbana, IL 61801, USA*

Received 6 April 1999; accepted 13 July 1999

Abstract

The fatigue performance of pure copper of the oxygen free, high conductivity (OFHC) grade and a dispersion strengthened copper alloy, Glid Cop™ CuAl-25 was examined with and without irradiation exposure. Mechanical testing was carried out to establish the fatigue lives of these materials in the unirradiated and irradiated states. Fatigue specimens of these two materials were irradiated with fission neutrons in the DR-3 reactor at Risø with a flux of $\approx 2.5\times10^{-17}$ n/m^2 s ($E>1$ MeV) to fluence levels of 1.5–2.5$\times10^{24}$ n/m^2 ($E>1$ MeV) at ≈47 and 100°C. Specimens irradiated at 47°C were fatigue tested at room temperature, whereas those irradiated at 100°C were tested at the irradiation temperature. These investigations demonstrated that, while irradiation causes significant hardening of the materials, the hardening appears to have no negative impact on fatigue performance. In fact, the fatigue performance of the CuAl-25 alloy is considerably better in the irradiated than that in the unirradiated state tested both at 22°C and 100°C. Microstructural observations of the fatigue microstructures and the fracture surfaces are useful in understanding this conclusion.

1. Introduction

The ITER design conditions require the use of high thermal conductivity materials for heat sink applications in first wall, limiter and divertor components and copper alloys provide the best potential for meeting these requirements. Fatigue behavior is central to materials selection since the vacuum vessel components will be subjected to thermal cycling, and thus thermal-mechanical cycling, as a result of the cyclic plasma burn operation of the system. Design requirements set the limits of useful fatigue testing in the range between around 10 to around 10^6 cycles to failure. Three alloys are currently under consideration including one dispersion strengthened (DS) alloy, Glid Cop CuA1-25, and two precipitation hardened (PH) alloys: CuCrZr and CuNiBe. The dispersion strengthened CuAl-25 alloy is the primary candidate alloy. The current work, which is part of a much larger experimental effort on a number of copper alloys [1,2], examines the fatigue performance of the dispersion strengthened alloy as compared to the performance of unalloyed copper in the form of oxygen free high conductivity (OFHC) Copper. The fatigue performance of these materials in the unirradiated condition at room temperature has been reported in earlier studies [3,4]. The current work centers on the influence of irradiation and test conditions up to 100°C.

2. Materials and experimental procedure

The materials used in the present investigations were oxygen free, high conductivity (OFHC) copper and dispersion strengthened Glid Cop™ CuAl-25 (LOCL). The OFHC-Cu was supplied by Tréfimétaux (France) in the form of 20 mm thick plates. The Glid Cop™ CuAl-25 (LOCL), hence forth referred to as CuAl-25, was supplied by OGM Americas (formerly SCM Metals, Inc.) in

* Corresponding author. Tel.: +45-46 775 709; fax: +45-46 775 758; e-mail: bachu.singh@risoe.dk

0022-3115/99/$ - see front matter
PII: S0022-3115(99)00188-9

the form of 15 and 20 mm diameter rods in the as-extruded (i.e. wrought) condition. The chemical composition and the thermo-mechanical treatments given to these materials prior to testing and irradiation are listed in Table 1. Values of the average grain size (d_g) of these materials are also quoted in Table 1.

The dislocation density in OFHC-copper was found to be rather low ($<10^{12}$ m^{-2}) [5]. In contrast, the CuAl-25 alloy in the as-wrought condition was found to contain a dislocation density of 1.5×10^{15} m^{-2} [5]. Most of these dislocations were associated with alumina particles. In addition to the dislocation structures in the CuAl-25 alloy, a reasonably high density of alumina particles (2.2×10^{22} m^{-3}) was present. The alumina particles were of ≈8.7 nm average diameter, but distributed very heterogeneously. Both particle size and density varied very considerably throughout the alloy [1,5]. The subsize fatigue specimens of OFHC-Cu and CuAl-25 were irradiated with fission neutrons in the DR-3 reactor at Risø at the reactor ambient temperature (≈47°C) and 100°C. All specimens were irradiated with a neutron flux of $\sim2.5\times10^{17}$ n/m^2 s ($E>1$ MeV) which corresponds to a displacement damage rate of $\approx5\times10^{-8}$ dpa (NRT)/s. The OFHC-Cu specimens received a fluence of $\approx2.5\times10^{24}$ n/m^2 ($E>1$ MeV) corresponding to a displacement dose level of ≈0.5 dpa. Specimens of CuAl-25 received a fluence of $\approx1.5\times10^{24}$ n/m^2 ($E>1$ MeV) corresponding to a displacement dose level of ≈0.3 dpa.

The main effect of irradiation with fission neutrons at ≈47°C was the introduction of interstitial-and vacancy-type defect clusters in high densities. A cluster density of $\approx5\times10^{23}$ m^{-3} was found in both OFHC-Cu and CuAl-25 irradiated with fission neutrons at ≈47°C to a dose level of 0.2 dpa [5].

Mechanical testing was carried out in an Instron machine with a specially constructed vacuum chamber where subsized fatigue specimens could be gripped and loaded. Fatigue tests were conducted primarily in a load controlled mode in an servo-electrical mechanical test stand. The characteristics of the loading cycle were monitored and controlled by computer. The loading cycles were always fully reversed (i.e. $R=-1$) so that the maximum tension load was the same as the maximum compressive load. The loading frequency was typically 0.5 Hz. The specimens tested in fatigue were cycled to failure, where failure was defined as separation of the specimen into two halves.

For elevated temperature testing, the specimens were heated by electrical resistance furnaces such that the heat was conducted through the specimen grips. This resulted in accurate temperature control and no measurable temperature gradient along the specimen length.

Following fatigue of both unirradiated and irradiated materials, fracture surfaces were examined in a JEOL 5310 low vacuum scanning electron microscope (SEM). For transmission electron microscopy investigations, 3 mm discs were cut from the gauge sections (close to the fracture surface) perpendicular to the fatigue axis. The discs were mechanically thinned to ≈0.1 mm and then twinjet electropolished in a solution of 25% perchloric acid, 25% ethanol and 50% water at 11 V for about 15 s at ≈20°C. The thin foils were examined in a JEOL 2000 FX transmission electron microscope.

3. Experimental results

3.1. Fatigue life evaluation

The fatigue performance of OFHC-Cu is indicated in Fig. 1 for unirradiated and 50°C irradiated specimens;

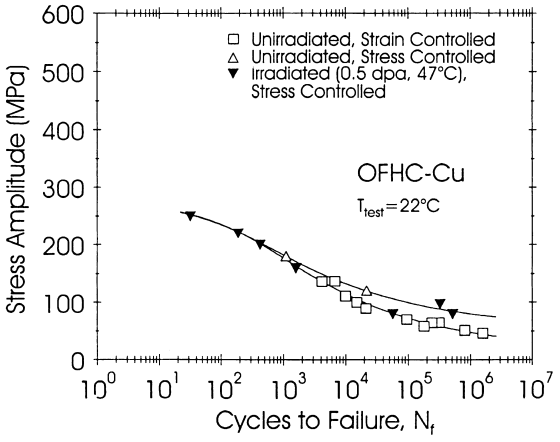

Fig. 1. Fatigue life (N_f) as a function of stress amplitude for unirradiated and irradiated OFHC-Cu tested at room temperature in vacuum. Irradiation was carried out at ≈47°C to a dose level of ~0.5 dpa (NRT). Note, that both stress- and strain-controlled tests give similar fatigue life, N_f. Furthermore, the fatigue life appears to increase due to irradiation.

Table 1
Chemical composition and thermomechanical treatments

Material	Composition	Thermomechanical processing
OFHC-Cu	Cu – 10, 3, <1, and <1 ppm of Ag, Si, Fe and Mg, respectively	Annealed at 550°C for 2 h in vacuum (<1.33 MPa): $d_g\approx100$ μm
CuAl-25	Cu – 0.25% Al as oxide particles (0.46% Al_2O_3)	As-supplied, i.e. as wrought, no subsequent heat treatment; $d_g<1$ μm

both types of specimens were tested at room temperature. The results suggest that the fatigue life of the irradiated specimens of OFHC-Cu may be longer than that of the unirradiated specimens at stress amplitudes lower than ≈150 MPa (i.e. at $N_f > 10^3$ cycles). However, in view of the limited number of results, this trend must be taken to be only tentative in nature. The comparison is further complicated by the fact that while unirradiated specimens were tested in the strain-controlled mode, all irradiated specimens were tested under stress control. It should be noted that the stress and the strain-controlled tests tend to yield similar results, particularly at lower cycles to failure. However, there are not enough results to confirm this trend.

The fatigue responses of CuAl-25 shown in Fig. 2, indicate a clear improvement in fatigue lives following irradiation to 0.3 dpa at 50°C as compared to the unirradiated condition. For most of the lives longer than about 500 cycles to failure, a modest increase in fatigue life over the unirradiated condition is found. The slopes of the fatigue curves appear to be nearly parallel in this region, but indicate about a factor of two increase in life for fixed load conditions. At short lives, the irradiated condition has a larger margin of life over the unirradiated condition. A comparison of the strain controlled and load controlled fatigue lives is also shown in Fig. 2 for unirradiated CuAl-25. The two sets of data match very closely. This indicates that the current load controlled tests are directly comparable to strain controlled tests; this issue will be addressed in more detail later. The CuAl-25 material shows an improvement in fatigue performance following irradiation and testing at 100°C (Fig. 3). In some cases, an improvement of nearly a factor of ten in fatigue lives at a fixed loading condition is found for the CuA1-25 in fatigue lives following irradiation to 0.3 dpa (Fig. 3).

A comparison of all of the fatigue results shown in Figs. 1–3 indicates that, for fixed loads, CuAl-25 provides the markedly better fatigue performance than OFHC-Cu.

3.2. Cyclic stress–strain evaluation

In order to provide useful information regarding the cyclic hardening or softening behavior of the two materials and to better correlate the results of stress-controlled and strain-controlled fatigue tests, a series of cyclic stress–strain curves were generated with cyclic step tests. In these tests, fully reversed fatigue loading was carried out at an initially low applied strain level, one in the elastic range. The specimen was cycled for a minimum of 20 cycles at the fixed strain range. The strain range was then increased by a small increment, and at least 20 cycles of loading were applied at each strain level while the load was monitored and recorded. Following stable or nearly stable cycling at each strain range, the strain range was increased by a small increment and the process repeated. Where possible, these tests were performed by first increasing the strain range incrementally to up to about 2% total strain and then decreasing the strain ranges back down in small increments to very low (i.e. elastic) strain ranges. This allowed for an analysis of residual hardening or softening which can take place during the loading cycles. Tests were performed on both unirradiated and irradiated materials. Examples of the cyclic stress–strain curves for OFHC-Cu are shown in Fig. 4 which demonstrates the

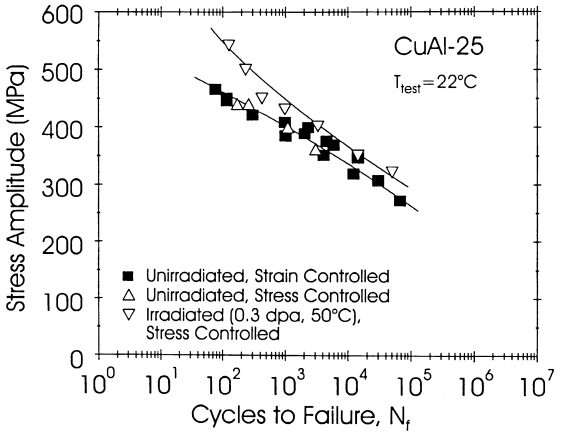

Fig. 2. Fatigue life (N_f) as a function of stress–amplitude for unirradiated and irradiated CuAl-25 alloy (in as-wrought condition) tested at room temperature in vacuum. Irradiation was carried out at ~47°C to a dose level of ~0.3 dpa. Note, that the fatigue life is not affected by the testing mode. It should be noted, however, that the neutron irradiation causes a significant increase in the fatigue life.

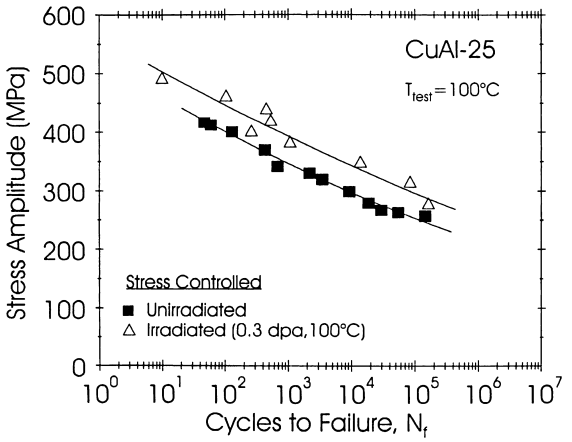

Fig. 3. Same as in Fig. 2, but irradiated and tested in vacuum at 100°C. Note, a significant improvement in fatigue life at all stress amplitudes.

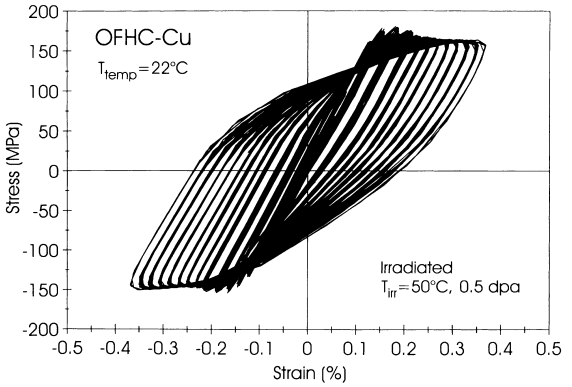

Fig. 4. Section of a cyclic stress–strain curve for OFHC-Cu irradiated at ≈47°C to a displacement dose level of ≈0.5 dpa and tested in the strain controlled mode at room temperature, showing the stress response in individual cycles. The progressive softening at each cycle at fixed loads can be seen.

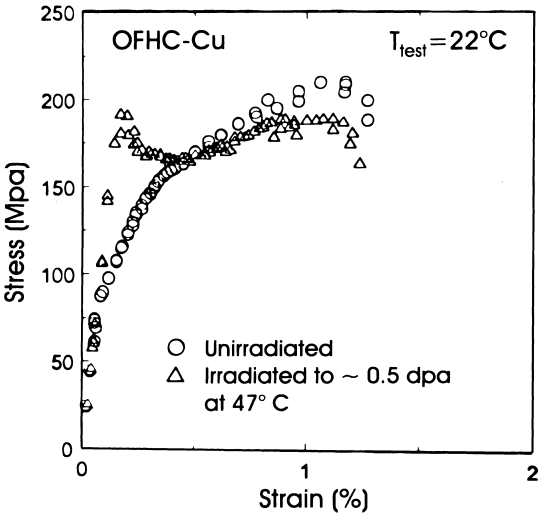

Fig. 5. Cyclic stress–strain curves for OFHC-Cu tested at room temperature in the unirradiated and irradiated (0.5 dpa at ~47°C) conditions. Note the occurrence of a prominent yield drop in the irradiated OFHC-Cu.

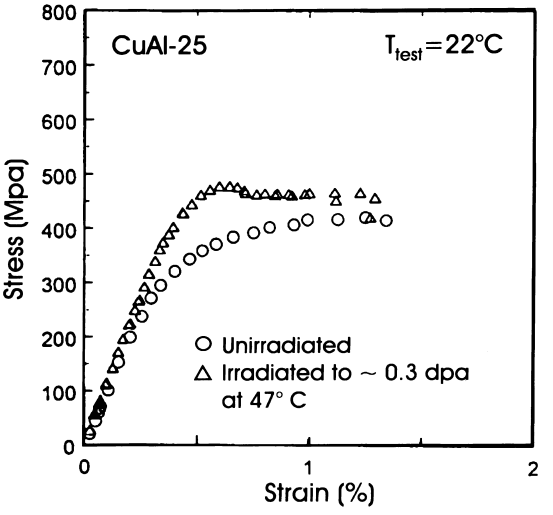

Fig. 6. Same as in Fig. 5, but for the CuAl-25 alloy in the unirradiated and irradiated (~0.3 dpa at 47°C) conditions. Note that the irradiated CuAl-25 does not exhibit a clear yield drop.

cycle by cycle softening behavior for loading conditions in the upper yield area on an irradiated specimen of OFHC-Cu specimen. It should be noted that the material is gradually softening during each loading cycle at any given applied strain range. Thus the final stress level at any given strain depends on the total number of cycles at that condition. The amount of softening per cycle at each strain level, however, does seem to decay to smaller values as the number of cycles increases. In any case, the tendency to cyclically soften is clear in all of the irradiated conditions.

The results of these tests are shown in Figs. 5 and 6 for OFHC-Cu and CuAl-25, respectively. These tests were carried out at room temperature. It can be noted that in all cases the irradiated materials exhibit a higher cyclic 'yield' point than do any of the unirradiated materials. In addition, there is an apparent upper and lower yield phenomenon similar to those seen in the monotonic tensile behavior of the irradiated specimens [5].

Following the initial post-yield drop in cyclic strength in the irradiated conditions, the balance of the cyclic stress–strain curves remains relatively flat, but at much reduced stress levels compared to the initial irradiation-hardened case. This post-yield drop in the cyclic strength is a clear indication of the softening effect induced by defect cluster removal by dislocation sweeping and localized deformation. In the cases of both of the alloys, a somewhat elevated strength persists as compared to the unirradiated curves. In the case of OFHC-Cu (Fig. 5), however, once the cyclic softening is induced, the curve very closely follows that of the unirradiated case. In other words, after the initial yield drop the OFHC-Cu shows clear evidence of work hardening. This is a significantly different behavior compared to the commonly observed behavior of irradiated copper during tensile tests, where plastic instability follows the yield drop and the material looses its ability to work harden [5–7].

The work reported here is based primarily on tests conducted under load control, where the specimen is cycled between fixed load limits. It is more common, where possible, to conduct low cycle fatigue tests in the strain controlled mode, where the specimen is cycled between fixed strain (extension) limits. The current work

indicates, however, that similar results are obtained from both test methods (see Figs. 1 and 2). In order to make the load controlled results more compatible and of broader use, the cyclic stress–strain curves are used to determine the cyclic hardening curves. The total cyclic strain can be represented as

$$\Delta\varepsilon_{\text{total}} = \Delta\varepsilon_{\text{elastic}} + \Delta\varepsilon_{\text{plastic}} = \Delta\sigma/E + (\Delta\sigma/K')^{1/n'}.$$

This formulation assumes the standard Ramberg–Osgood-type relationship for strain hardening in the plastic regime, where K' is the cyclic strength coefficient, n' the cyclic strain hardening exponent. The original formulation was applied to strain hardening under monotonic loading conditions such that

$$\varepsilon_{\text{total}} = \varepsilon_{\text{elastic}} + \varepsilon_{\text{plastic}} = \sigma/E + (\sigma/K)^{1/n},$$

where K is the strength coefficient and n the strain hardening exponent. These relationships, while empirical, provide an excellent representation of the material deformation behavior from the elastic regime through a large portion of the post-yield response for a wide variety of metals and alloys. These relationships provide a useful constitutive relationship, where the applied stress or stress amplitude, at any point in the loading can be directly correlated with a unique strain or strain range. Once the constants in either equation have been determined, it is straightforward to convert stresses (or loads) to strain and vice versa.

In the current study, the cyclic stress–strain curve provides the means for determining the relevant constants. The stress (or load) based fatigue life curves can be converted to strain-based information using the above equation once the values of the constants have been determined. The values of the current constants are given in Table 2. Figs. 7 and 8 show the elastic strain range only, and cyclic hardening results for converting the load controlled tests to strain versus life curves. The conversions are compared to previous strain-controlled tests.

Figs. 7 and 8 indicate the viability of converting fatigue performance based on load (stress) controlled tests to the more common strain-life representation. This is accomplished by either using strains calculated from the elastic modulus, E, or strain calculated from the plastic strain hardening coefficient, K or K', and the strain hardening exponent, n or n'. In the case of the OFHC-Cu, the fits are very good. The case of CuAl-25 is somewhat more complicated; the comparisons are not as satisfactory as for the case of OFHC-Cu. It should also be noted here, that most of the fatigue life data fall into the regime, where both the elastic and plastic strain contributions are important. The elastic strain predictions are close to the elastic portion of the strain range, whereas the plastic or cyclic hardening conversions lie

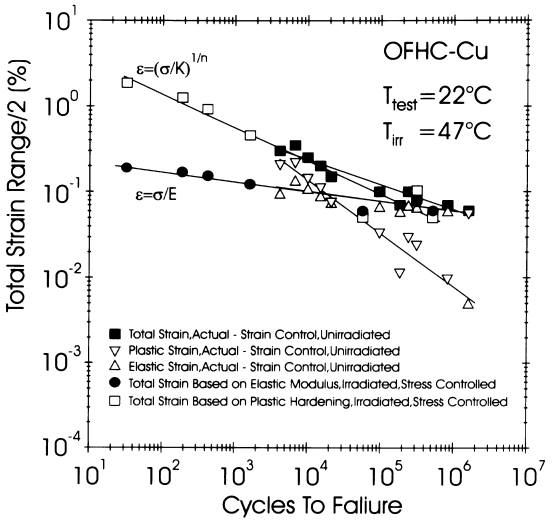

Fig. 7. Fatigue life (N_f) as a function of the measured and calculated (from cyclic stress–strain curves) strains for the unirradiated and irradiated (0.5 dpa at ≈47°C) OFHC-copper tested at 22°C.

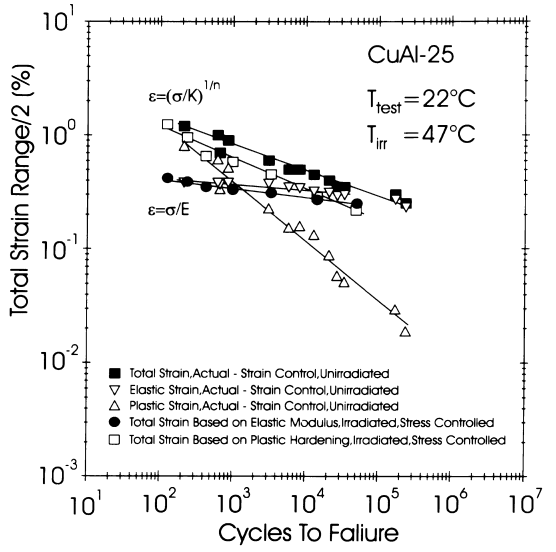

Fig. 8. The same as in Fig. 7, but for CuAl-25 irradiated (0.3 dpa at 47°C) and tested at 22°C.

Table 2
Monotonic and cyclic strength coefficients and hardening exponents for unirradiated conditions

Material	Monotonic		Cyclic	
	K	N	K'	n'
OFHC-Cu	53.4	0.356	205.3	0.318
CuAl-25	358.9	0.525	509	0.303

substantially above the actual plastic strain curve, but marginally below the actual total strain–life curve for unirradiated material. This indicates that some caution must be taken in this case, at least, when converting from fatigue life data taken from stress controlled tests to strain-based formulations.

3.3. Characterization of fatigue-induced microstructural evolution

The post-fatigue microstructure of OFHC-Cu tested at room temperature in the unirradiated condition is dominated by equiaxed and elongated cells. At the high load level (180 MPa, $N_f = 1121$) the cell formation occurs throughout the entire specimen. However, the cell formation occurs in an inhomogeneous fashion in that the cells in some areas are equiaxed and in other areas narrow and elongated (Fig. 9). At the low load level of 120 MPa ($N_f = 21646$), most of the cells are narrow and elongated, but some areas of the specimen contain loose dislocation walls and very long cells.

The microstructural evolution in the irradiated specimens of OFHC-Cu during fatigue testing is found to be substantially different from that observed in the unirradiated OFHC-Cu. A general comparison of the microstructural features of unirradiated and irradiated conditions is given in Table 3. The post-fatigue microstructure in the irradiated specimens is rather complex and varies significantly with the stress amplitude. Fig. 10 illustrates selected features of the post-fatigue microstructure of the irradiated OFHC-Cu for stress amplitudes from 80 to 250 MPa. At the highest stress amplitude of 250 MPa ($N_f = 32$), the microstructure is found to contain small cells with loose dislocation walls,

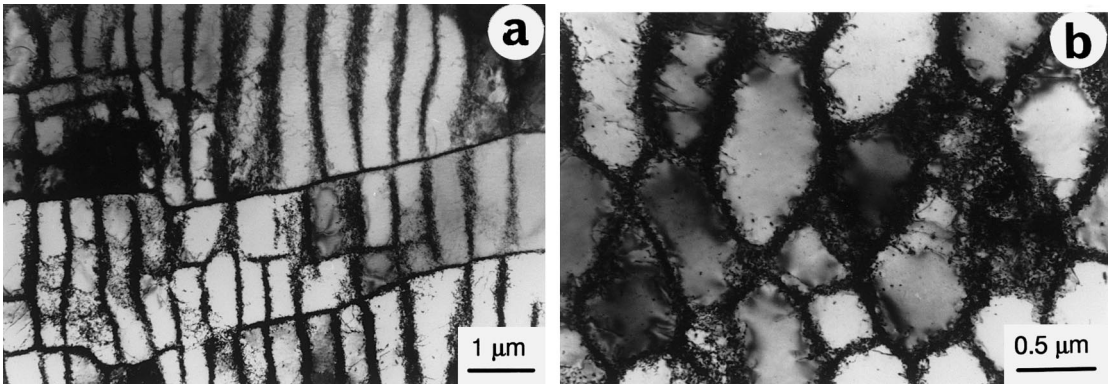

Fig. 9. Post-fatigue microstructure of the unirradiated OFHC-Cu tested at room temperature showing formation of equiaxed and elongated cells: (a,b) 180 MPa, $N_f = 1121$.

Table 3
Comparison of microstructural observations in fatigue tested (at room temperature) OFHC-Cu with and without irradiation exposure

N_f	σ (MPa)	Microstructure
Unirradiated		
1121	180	Mixture of equiaxed and very elongated cells
21646	120	Microstructure dominated by elongated cells – in some cases with loose walls; very elongated cells only in some areas
Irradiated (47°C, 0.5 dpa)		
32	250	Complicated microstructure containing: • Small cells with loose dislocation walls • Slip bands and 'cleared' channels • Areas with defect clusters and grown-in dislocations
189	220	Mostly equiaxed cells but some areas contain homogeneous distribution of dislocations
424	200	Mostly equiaxed cells; however, some areas contain 'cleared' channels. Areas were also found where the as-irradiated microstructure had survived and where no dislocations were generated
1604	160	Tendency to form cells with loose walls, homogeneous distribution of dislocations, clusters appear to have been wiped out.
515988	80	No sign of extensive global plastic deformation, defect clusters are seen everywhere, bands of dislo-cations, no indication of cell formation

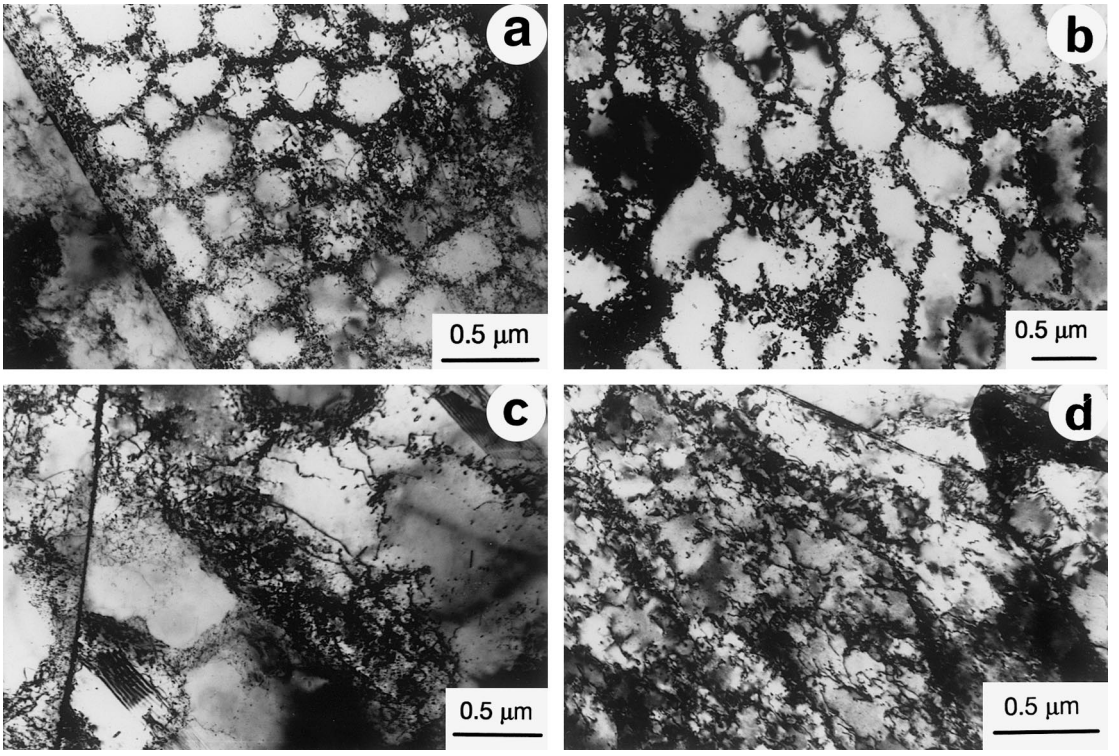

Fig. 10. Post-fatigue microstructure of the OFHC-Cu irradiated at 47°C to 0.5 dpa and tested at room temperature at different stress amplitudes: (a) 250 MPa ($N_f = 32$), (b) 200 MPa ($N_f = 424$), (c) 160 MPa ($N_f = 1604$) and (d) 80 MPa ($N_f = 56634$).

slip bands, and 'cleared' channels. The interior of the cells and the slip bands (Fig. 10(a)) contain very few or no defect clusters produced during irradiation. A clear example of 'cleared' channels is shown in Fig. 11. It should be noted here that in the regions away from the cleared channel there is no evidence of dislocation generation during the cyclic deformation even at the stress level of as high as 250 MPa. This is consistent with the lack of dislocation generation in the irradiated OFHC-Cu tensile tested at room temperature [5].

Fig. 10(b) shows the microstructure observed in the irradiated specimens of OFHC-Cu following cyclic deformation at a stress amplitude of 200 MPa ($N_f = 424$). A mixture of equiaxed and elongated cells can be seen in Fig.10(b). Again, the cells contain very few or no defect clusters.

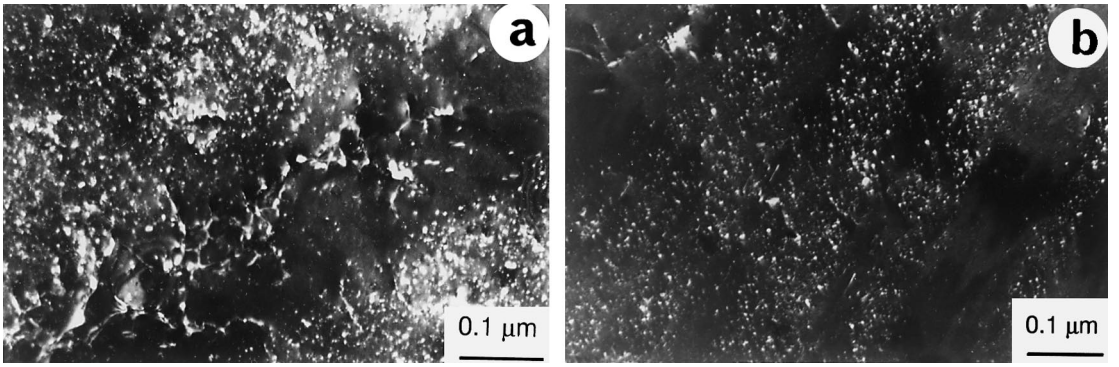

Fig. 11. An example of 'cleared' channels formed in the OFHC-Cu irradiated at 47°C to 0.5 dpa and fatigue tested at room temperature at a stress amplitude of 200 MPa ($N_f = 424$). Similar channels were also observed at the stress amplitude of 250 MPa ($N_f = 32$). Note the lack of dislocation generation in regions between the 'cleared' channels.

The fatigue-induced microstructure of irradiated OFHC-Cu tested at a stress amplitude of 160 MPa ($N_f = 1604$) is shown in Fig. 10(c). At this stress level, although there is a tendency towards cell formation, but the formation of proper cells is not completed. The microstructure is dominated, instead, by the high density of fatigue-induced dislocations with a reasonably homogeneous distribution. At this test condition, there is a tendency for dislocations to segregate in the form of loose bands. It is significant that at the stress amplitudes of 160 MPa and below, elongated cells and very long dislocation walls or veins are not formed. This would suggest that both generation and the mobility of dislocations were seriously reduced in the irradiated materials.

At the stress amplitude of 80 MPa, there is no indication of formation of cells and subgrains (Fig. 10(d)). However, as can be seen, dislocations have a tendency to cluster, segregate and form bands of dislocations.

The post-fatigue microstructures of the CuAl-25 alloy in the unirradiated and irradiated conditions are shown in Figs. 12–14 and the main features are summarized in Table 4. The most significant aspect of these observations is that the overall activities of dislocations (generation, interactions and segregation) are drastically reduced in CuAl-25 compared to that in the OFHC-Cu. At the stress amplitude of 440 MPa ($N_f = 262$), there is a tendency to form some very small (100–200 nm diameter) and rather loose cells (Fig. 12(a)) in some parts of the specimens. Generally, the microstructure is dominated by the presence of small dislocation segments pinned probably by the oxide particles (Fig. 12(b)). No indication of cell formation was observed in the unirradiated CuAl-25 fatigue tested at a stress amplitude of 360 MPa (Fig. 13). Fig. 14 shows the dislocation microstructure of the irradiated CuAl-25 after fatigue testing at stress amplitudes of 540 MPa (Fig. 14(a)) and 320 MPa (Fig. 14(b)). No indication of cell formation

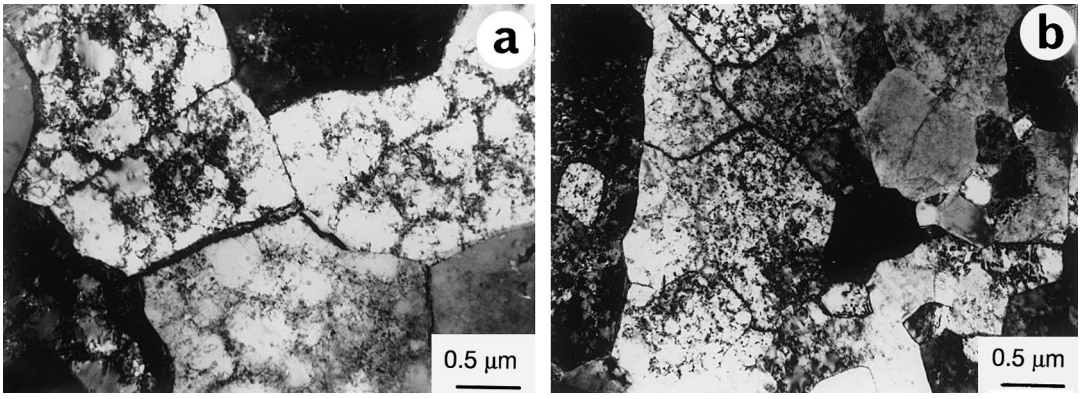

Fig. 12. Post-fatigue microstucture of the unirradiated CuAl-25 alloy tested at room temperature at a stress amplitude of 440 MPa ($N_f = 262$): (a) small cells with loose dislocation walls and (b) rather homogeneous distribution of dislocations.

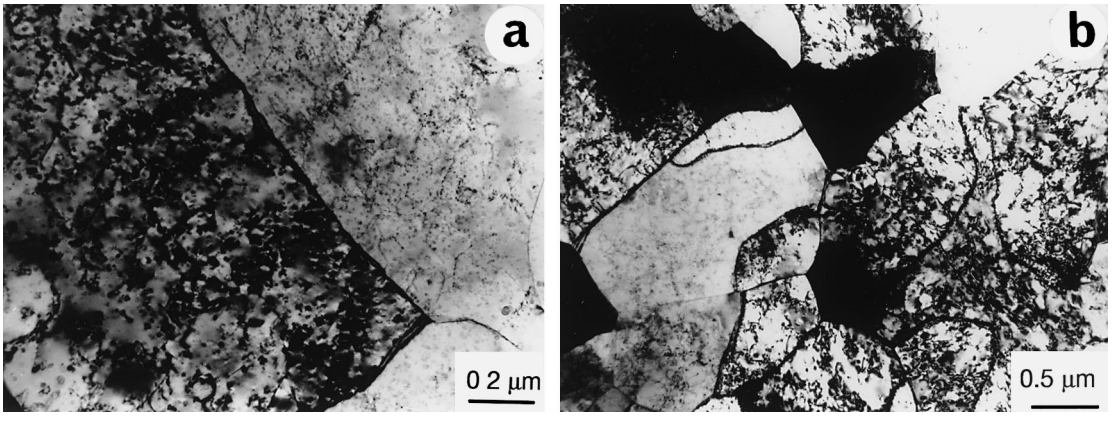

Fig. 13. Same as in Fig. 12, but tested at a stress amplitude of 360 MPa ($N_f = 2994$) showing homogeneous distribution of dislocations at (a) low and (b) high magnification. Note, the lack of long-range dislocation transport and interaction.

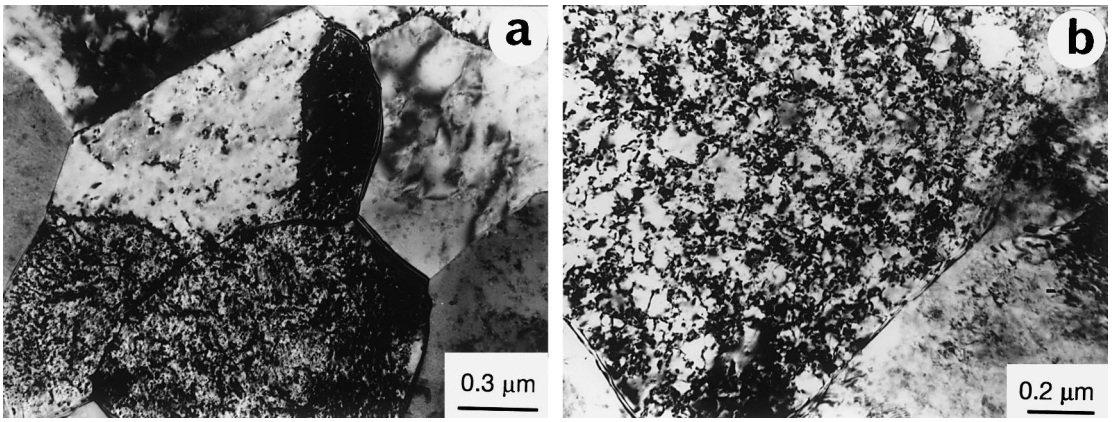

Fig. 14. Post-fatigue microstructure of the irradiated (0.3 dpa, 47°C) CuAl-25 alloy tested at room temperature at a stress amplitude of (a) 540 MPa ($N_f = 129$) and (b) 320 MPa ($N_f = 49506$). At the stress amplitude of 320 MPa there appears to be no evidence of dislocation generation and migration.

Table 4
Comparison of microstructural observations in fatigue tested (at room temperature) glidcop CuAl-25 with and without irradiation exposure

N_f	σ (MPa)	Microstructure
Unirradiated		
262	440	Dislocation generation, interactions and tendency to form small (100–200 nm) loose cells
2994	360	Homogeneous distribution of dislocations in the grains
Irradiated (47°C, 0.3 dpa)		
129	540	High density of homogeneously distributed dislocations, most of the defect clusters appear to have been wiped out or at least they are not visible
247	500	High dislocation density, tendency to form small (~200 nm) loose cells, defect clusters appear to have been wiped out
3235	400	Density of dislocations generated by deformation rather low, no indication of cell formation, not all the grains appear to have deformed plastically (these undeformed grains still contain as-irradiated defect clusters and dislocation microstructure)
49506	320	Only a few grains appear to have deformed plastically and a large number of grains still contain as-irradiated cluster and dislocation microstructure

was observed in these specimens. In the specimen tested at 320 MPa not all the grains seem to have deformed plastically; a large number of grains still contain as-irradiated cluster and dislocation microstructures. The lack of dislocation generation during the fatigue experiment at 320 MPa can be seen in Fig. 14(b).

3.4. Fracture surface analysis

The fracture surfaces of the fatigue specimens were examined by SEM to identify significant features that could relate to the fatigue performance. A comparison of the macroscopic features of the unirradiated and irradiated fracture surfaces is shown in Fig. 15 for OFHC-Cu and in Fig. 16 for CuAl-25. A comparison of the irradiated and unirradiated conditions indicates that, while the fracture surfaces are reasonably flat in the case of unirradiated materials, the irradiated conditions indicate a significant amount of necking during the final stages of fatigue loading. This is thought to be directly related to the cyclic hardening in the unirradiated materials which should not lead to necking, and the cyclic softening in the case of irradiated materials which could lead to necking. This should also be evident from the upper yield point phenomenon shown by the cyclic stress–strain curves for the irradiated materials.

A closer examination of the failure surfaces provides more information regarding the nature of the fractures. A comparison of the unirradiated and irradiated OFHC-Cu fracture surfaces indicates that in the unirradiated condition specimens failed by the classic fatigue crack initiation and growth mechanism. The fatigue striations are clearly evident on the failure surfaces

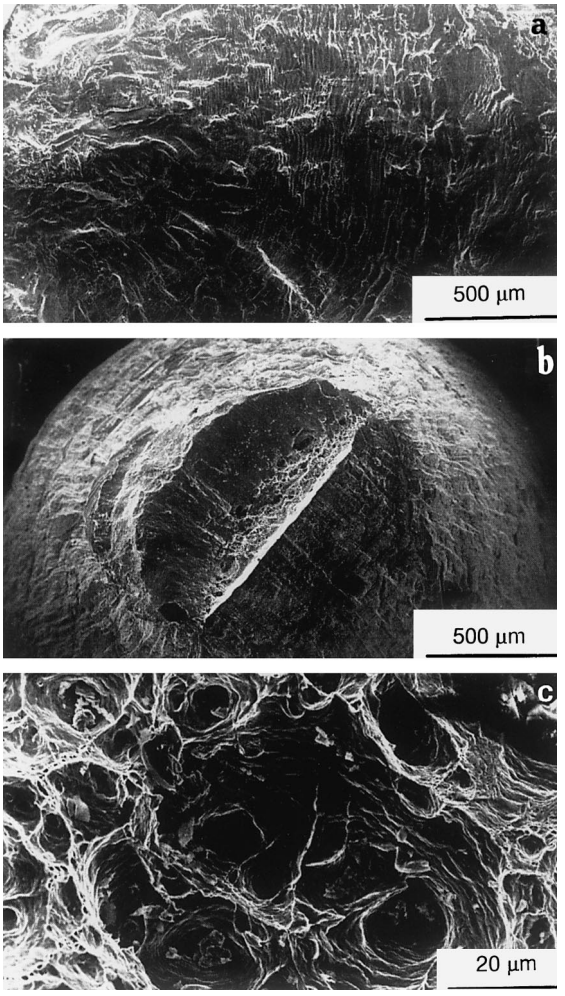

Fig. 15. SEM fractographs of the fracture surfaces of fatigue tested OFHC-copper at 22°C in (a) unirradiated ($N_f = 1121$), (b) irradiated (47°C, 0.5 dpa, $N_f = 32$) conditions, and (c) same as (b), but at a higher magnification showng extensive deformation.

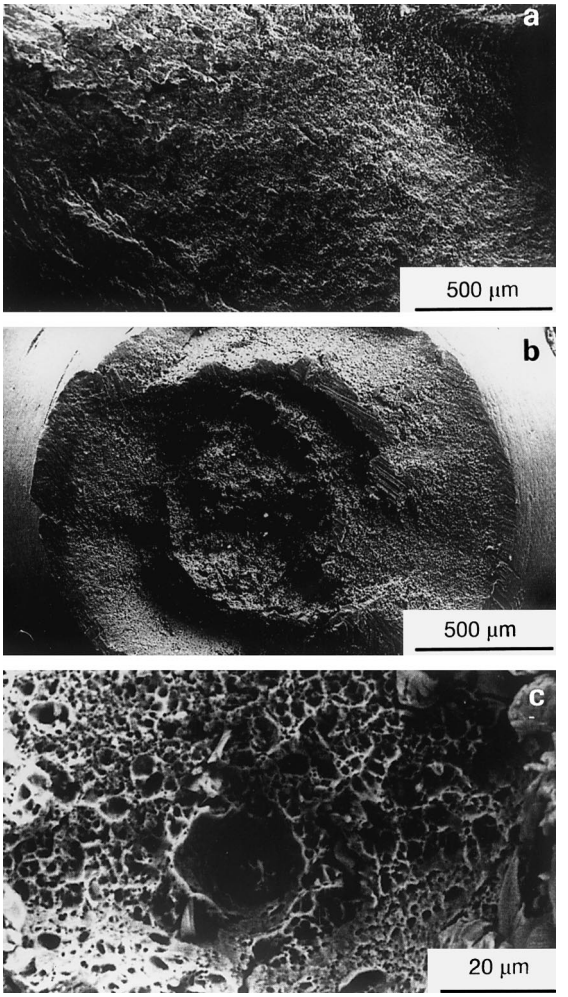

Fig. 16. SEM fractographs of the fracture surfaces of fatigue tested CuAl-25 at 22°C in (a) unirradiated ($N_f = 262$), (b) irradiated (47°C, 0.3 dpa, $N_f = 129$) conditions, and (c) Same as (b), but at a higher magnification showing a large amount of plasticity-induced deformation voids.

indicating that the crack advanced through the specimen with little redistribution of plasticity. No secondary cracking or other crack branching is evident. On the contrary, the irradiated material shows extensive deformation up to the point of separation (Fig. 15(c)), which is also a result of ductile fracture. The clear indication of intersection of flow lines over the entire material surface indicates the extent to which plastic deformation is distributed around the neck region.

By somewhat of a contrast, the failure surfaces of the unirradiated and irradiated CuAl-25 are rather similar. In both cases the evidence of secondary cracking is observed. While necking is seen in the irradiated conditions, the nature of the final fracture surfaces is microscopically similar. A limited amount of plastic deformation induced void formation is apparent and the final failures appear to be relatively ductile in nature. The ductility, however, is constrained to this very large population of voids, which appears to be associated with the alumina particle distributions (Fig. 16(c)).

4. Discussion

Since neutron irradiation causes a drastic decrease in the uniform elongation of copper and copper alloys [6–8], the possibility that the neutron irradiation may also impair the fatigue performance of these materials cannot be ruled out. The present results strongly suggest,

however, that this may not be the case at 50°C and 100°C. In fact, the results for the CuAl-25 alloy show just the opposite in that the irradiation improves the fatigue lifetime both at room temperature and 100°C when tested in the post-irradiation condition.

The results of the low cycle fatigue experiments carried out on OFHC-Cu and CuAl-25 both in the unirradiated and irradiated conditions have demonstrated two significant features of the effect of irradiation on their performance. First, the irradiated materials exhibit a yield drop and softening during the first few cycles of fatigue experiments. In the case of irradiated OFHC-Cu, the yield drop is followed by hardening at higher fatigue cycles. Second, the fatigue life of the irradiated materials tested at 22°C is noticeably improved by irradiation (Figs. 1–3). The fact that the effect of irradiation on fatigue life is relatively innocuous or even positive is of academic as well as of technological interest (e.g. for the lifetime of components in ITER). In the following, both of these issues are discussed particularly in terms of the results of microstructural investigations and fracture surface analyses.

Let us first consider the origin and implications of the initial yield drop (cyclic softening) followed by hardening or hardening and plastic instability in the irradiated OFHC-Cu and CuAl-25. It is relevant to note here that the initial yield drop is a matter of common observations in copper irradiated and tensile tested at temperatures below the recovery stage V (i.e. $<0.3\ T_m$, where T_m is the melting temperature) to a dose level of about 0.1 dpa or higher (e.g. [5–7]). The occurrence of a prominent yield drop in a pure fcc metal is, however, highly unusual. Generally, the yield drop is a characteristic deformation feature of the bcc metals containing interstitial impurities (e.g. carbon and nitrogen in iron). It is well established that the impurity atoms segregate at the dislocations and prevent them from acting as Frank–Read sources. At the upper yield stress, a large number of dislocations break away from the atmosphere of the impurity atoms, causing a yield drop. This is consistent with the theoretical prediction that a prominent yield drop is likely to occur when the density of unlocked dislocations is very low (10^6–10^8 m^{-2}) [8]. This clearly suggests that the grown-in dislocations in copper must get locked during irradiation and it is their release at the upper yield stress that causes the yield drop. The question then arises as to how the grown-in dislocations get locked during irradiation?

This question has been addressed recently in a new model for radiation hardening called 'Cascade Induced Source Hardening' (CISH) [9]. In this model, the grown-in dislocations are taken to be decorated by small loops of self-interstitial atoms (SIAs). The upper yield stress is the stress necessary to pull the dislocation away from the atmosphere of loops surrounding the grown-in dislocations. It has been further shown that the decoration is caused by the one-dimensional glide of small SIA loops/clusters produced in the cascades [10]. The experimental evidence showing the decoration of grown-in dislocations by SIA loops is reviewed in [10].

Thus, the observed yield drop behaviour in copper and copper alloys can be understood in terms of the CISH model. The fact that the yield drop in the case of the CuAl-25 alloy is very small can be easily rationalized in terms of the high density of grown-in dislocations (1.5×10^{15} m^{-2} [5]) and the presence of dispersions of hard Al_2O_3 particles acting as strong obstacles to dislocation motion. In the case of CuAl-25, most of the grown-in dislocations (introduced during manufacturing process) are associated with Al_2O_3 particles and thereby strongly locked. During deformation, even if some of the dislocations are unlocked at the upper yield stress, they cannot move long distances because Al_2O_3 particles will block their motion.

In this context, it is worth pointing out that the post-fatigue microstructures observed in the irradiated OFHC-Cu and CuAl-25 provide an overwhelming amount of evidence for a very efficient removal of the irradiation-induced defect clusters by the dislocations generated during the cyclic loading. Once the dislocations are generated, they move under the influence of applied stress and wipe out practically all defect clusters in their path by elastic force field interactions between small loops and gliding dislocations. This implies that the irradiation-induced defect clusters do not act as strong obstacles to the dislocation motion and therefore are unlikely to be the cause of the observed hardening [9]. Instead, the irradiation produced cascades render the generation of dislocations more difficult or impossible by inducing decoration of the grown-in dislocations by small loops. This leads to an increase in the upper yield stress and inhomogeneous and localized deformation and gives rise to yield drop and plastic instability. This explains the observation of prominent necking during cyclic loading of the irradiated OFHC-Cu. The corresponding unirradiated specimens tested under the same condition, on the other hand, do not exhibit neck formation.

In view of the complicated nature of the deformation processes operating under cyclic loading conditions, it is not possible at present to provide a simple explanation for the observed lack of deleterious effects, and even a positive effect (i.e. increase in lifetime) of irradiation on fatigue lifetime, particularly in the case of the CuAl-25 alloy. It is important to recognize here that while the unirradiated copper and copper alloy deform homogeneously (i.e. without necking), the deformation in the irradiated materials is dominated by localized deformation producing prominent necking (Fig. 10). It should be pointed out that the necking is prominent only in the OFHC-Cu, but not in the case of the irradiated CuAl-25.

This difference in the deformation behavior between the unirradiated and irradiated states makes the comparison of their lifetime rather questionable. Furthermore, it is reasonable to speculate that the observed yield drop and necking may be due to the fact that fatigue experiments are conducted in the stress-controlled mode. The strain-controlled test, on the other hand, may prevent the localization of deformation and necking. This may yield a longer lifetime. In other words, the stress-controlled fatigue tests may underestimate the lifetime which may be achieved under the condition, where the cyclic loading may correspond to the strain controlled experiments (e.g. in the first wall and divertor components in ITER).

The fatigue lifetime improvement exhibited by the irradiated specimens of CuAl-25 both at 22°C and 100°C (Figs. 2 and 3) is consistent with the line of argument presented above. The irradiated CuAl-25 alloy, for instance, does not suffer from a prominent yield drop and extensive necking and yields a significantly longer lifetime in the whole range of the stress amplitudes used in the present experiments both at 22°C and 100°C. It should be pointed out that the irradiated CuAl-25 does not suffer from the yield drop during tensile testing at 22°C [5,7] either.

The post-fatigue microstructural investigations of the irradiated CuAl-25 alloy demonstrate two significant features: (a) difficulty in dislocation generation and (b) the lack of fatigue-damage accumulation in the form of large elongated cells or subgrains. These observations are consistent with the results of the cyclic stress–strain experiments (Fig. 6). These results suggest that although the alumina particles in the CuAl-25 alloy are strong obstacles to dislocation motion, the irradiation-induced decoration of the grown-in dislocations is still efficient in preventing dislocation generation.

It should be recognized though that this irradiation-induced improvement in the fatigue performance may not occur in the in-situ experiments corresponding to the service conditions of ITER. Under the dynamic conditions of ITER, it may be difficult, or even impossible, to decorate the grown-in dislocations by small SIA loops, because of the low displacement dose per burn-up cycle. In other words, the dislocation generation during the cyclic deformation under irradiation may occur in the same manner as in the case of unirradiated materials. Hence, an improvement in the fatigue lifetime may not occur. On the other hand, since the mobile dislocations under the dynamic conditions will keep removing the defect clusters produced by the cascades, the irradiation may not cause any deleterious effects on fatigue life either. It may be of interest, therefore, to carry out post-irradiation fatigue experiments on specimens irradiated to low doses (e.g. $\sim 10^{-2}$ dpa), particularly on CuAl-25 alloy, where the positive effect of alumina particles on dislocation generation and motion still may be maintained.

5. Summary and conclusions

In the present work, the low cycle fatigue behavior of the annealed OFHC-Cu and dispersion strengthened CuAl-25 has been investigated before and after these materials were exposed to neutron irradiation. Both materials were irradiated at ≈47°C and tested at 22°C. In addition, the CuAl-25 alloy was irradiated and tested at 100°C. The unirradiated specimens were tested both in stress- and strain-controlled modes, whereas all irradiated specimens were tested only in the stress-controlled mode. In order to determine the cyclic hardening or softening behavior of these alloys and to establish a correlation between the results of the stress-controlled and strain-controlled fatigue tests, a series of cyclic stress–strain curves were generated with cyclic step tests. To facilitate a better understanding of the mechanical performance of these materials, the microstructure and fracture surfaces were investigated in detail using transmission and scanning electron microscopy.

On the basis of the results of the mechanical testing and microstructural investigations, the following main conclusions may be drawn:

1. The unirradiated specimens tested at 22°C in the stress- and strain-controlled modes exhibit similar fatigue life.
2. The cyclic step tests clearly demonstrate that the irradiated specimens of OFHC-Cu suffer from a prominent yield drop; the irradiated CuAl-25 specimens, on the other hand, do not exhibit such a prominent yield drop.
3. All unirradiated specimens deform homogeneously, whereas irradiated specimens of both OFHC-Cu deform inhomogeneously and exhibit extensive necking during fatigue experiments. The amount of necking observed in the irradiated CuAl-25 specimens is very limited.
4. Irradiated specimens of OFHC-Cu and CuAl-25 exhibit a noticeable improvement in the fatigue performance due to irradiation. This improvement is quite significant in the case of CuAl-25 both at 22°C and 100°C.
5. The use of cyclic step tests to generate cyclic stress–strain curves is a useful means of comparing the effects of cyclic loading to monotonic (tensile) loading, and to generate a cyclic strength coefficient, K', and cyclic hardening exponent, n', which are useful for interpreting load control vs. strain control fatigue life data.
6. The data analysis based on cyclic strain hardening behavior allows for conversion of fatigue life information from load control tests to strain-based correlations. This conversion must be used with some care, however, particularly when trying to compare data from irradiated tests and unirradiated tests which are obtained with different test control conditions. Nevertheless, the information provides useful

guidance for interpreting stress controlled test data when design conditions may require strain-based information.

7. The observed post-fatigue microstructures indicate that the difficulty in the generation of fresh dislocations during fatigue deformation limits the scale of the fatigue damage accumulation and may be responsible for the improvement in the observed fatigue lifetime. In the case of CuAl-25, the presence of Al_2O_3 particles makes further contribution to this improvement by acting as strong obstacles to dislocation motion.
8. The irradiation-induced defect clusters do not appear to act as effective obstacles to dislocation motion during fatigue deformation; once generated, the mobile dislocations wipe out the irradiation-induced defect clusters. A similar behavior has been observed in the irradiated and tensile tested specimens of OFHC-Cu.
9. The analysis of the present results suggests, however, that the irradiation-induced improvement in the fatigue lifetime observed in the post-irradiation tests may not occur during the service condition of ITER, where the accumulated damage in one burn-up cycle may not be high enough to decorate the grown-in dislocations (by small SIA loops) and render them immobile. On the other hand, since the mobile dislocations generated during cyclic deformation are quite effective in removing the irradiation-induced defect clusters, the irradiation may not cause deleterious effects on the fatigue lifetime of these materials.
10. It is suggested that the post-irradiation fatigue testing of specimens irradiated to low doses ($<10^{-2}$ dpa) may be useful in verifying the above conclusion, particularly in the case of CuAl-25 alloy.

Acknowledgements

The present work was partly funded by the European Fusion Technology Programme. The authors would like to thank B.F. Olsen and J.L. Lindbo for the technical assistance.

References

[1] B.N. Singh, D.J. Edwards, M. Eldrup, P. Toft, Risø-R-937 (EN), January 1997.
[2] B.N. Singh, D.J. Edwards, M. Eldrup, P. Toft, Risø-R-971 (EN), February 1997.
[3] A. Singhal, J.F. Stubbins, B.N. Singh, F.A. Garner, J. Nucl. Mater. 212–215 (1994) 1307.
[4] K.D. Leedy, J.F. Stubbins, B.N. Singh, F.A. Garner, J. Nucl. Mater. 233–237 (1996) 547.
[5] B.N. Singh, D.J. Edwards, P. Toft, J. Nucl. Mater. 238 (1996) 244.
[6] S.A. Fabritsiev, S.J. Zinkle, B.N. Singh, J. Nucl. Mater. 233–237 (1996) 127.
[7] B.N. Singh, A. Horsewell, P. Toft, D.J. Edwards, J. Nucl. Mater. 224 (1995) 131.
[8] G.T. Hahn, Acta Metall. 10 (1962) 727.
[9] B.N. Singh, A.J.E. Foreman, H. Trinkaus, J. Nucl. Mater. 249 (1997) 103.
[10] H. Trinkaus, B.N. Singh, A.J.E. Foreman, J. Nucl. Mater. 249 (1997) 91.